STATISTICAL SHAPE MODELS FOR SEGMENTATION AND STRUCTURAL ANALYSIS

Guido Gerig, Martin Styner

Department of Computer Science
University of North Carolina
Chapel Hill, NC 27514, USA
gerig@cs.unc.edu

Gábor Székely

Swiss Federal Institute of Technology
Communication Technology Laboratory
ETH-Zentrum, CH-8092 Zurich,
Switzerland

ABSTRACT

Biomedical imaging of large patient populations, both cross-sectionally and longitudinally, is becoming a standard technique for noninvasive, in-vivo studies of the pathophysiology of diseases and for monitoring drug treatment. In radiation oncology, imaging and extraction of anatomical organ geometry is a routine procedure for therapy planning an monitoring, and similar procedures are vital for surgical planning and image-guided therapy. Bottlenecks of today's studies, often processed by labor-intensive manual region drawing, are the lack of efficient, reliable tools for three-dimensional organ segmentation and for advanced morphologic characterization.

This paper discusses current research and development focused towards building of statistical shape models, used for automatic model-based segmentation and for shape analysis and discrimination. We build statistical shape models which describe the geometric variability and image intensity characteristics of anatomical structures. New segmentations are obtained by model deformation driven by local image match forces and constrained by the training statistics. Two complimentary representations for 3D shape are discussed and compared, one based on global surface parametrization and a second one on medial manifold description. The discussion will be guided by presenting a most recent study to construct a statistical shape model of the caudate structure.

1. INTRODUCTION

This paper discusses two complimentary shape representation schemes for three-dimensional objects, a parametric boundary description using spherical harmonics (SPHARM) and a medial manifold description (skeletonization) using a sampled medial representation (M-rep). Both representations can describe the same objects but are fundamentally different in the way they represent the object shapes.

The SPHARM description (see Brechbühler [1, 2]) is a *global, fine scale description* that represents shapes of spherical topology. The basis functions of the parameterized surface are spherical harmonics. SPHARM is a smooth, accurate surface shape representation given a sufficiently small approximation error (see Fig. 1a). Based on a uniform icosahedron-subdivision of the spherical parameterization, a Point Distribution Model (PDM) is directly obtained from the coefficients via a linear mapping between parameter space and image coordinates. Correspondence of surface points represented by SPHARM is determined by normalizing the parameterization and the object alignment to the coarse shape represented by the first order, which is an ellipsoid. Truncating the spherical harmonic series at different degrees results in object representations at different levels of detail, resulting in a multi-scale object representation.

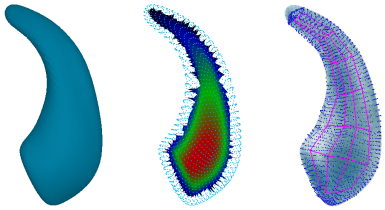

Fig. 1. Alternative shape representation schemes to characterize a three-dimensional caudate structure: a) boundary representation parametrized by spherical harmonics (SPHARM, fine-scale), b) skeletal representation based on a pruned Voronoi diagram and color coding of the local radius of enscribed spheres (local, fine-scale), and c) sampled medial description (mesh of atoms) with implied boundary (local, coarse scale). Pictures show average models from a population of 186 objects.

The discrete, sampled medial representation (M-rep) is a discrete, local medial shape description. It is a set of linked samples, called medial atoms, $m = (\vec{x}, r, \underline{F}, \theta)$ (see Pizer,Joshi et al. [3, 4]). Each atom is composed of: 1) a position $\vec{x}$, 2) a width r, 3) a frame $\underline{F}$ implying the tangent plane to the medial manifold and 4) an object angle θ. A

figure is a non-branching medial sheet. Multiple figures are connected via inter-figural links. The medial atoms form a graph with edges representing either inter- or intra-figural links. In the generic case, this medial graph is non-planar, i.e. overlapping when displayed in a 2D diagram. The sampling is sparse and leads to a coarse scale description (see Fig. 1c). Correspondence between shapes is implicitly given if the medial graphs are equivalent. The medial graph at each sampling scale implies an object boundary, thus representing objects at a hierarchy of scales.

Both shape representations are used in automatic segmentation methods by model deformation, driven by local boundary match forces but constrained by global smoothness and statistical geometric object priors. Further, parameterizations of three-dimensional objects and object populations are used for describing statistics of healthy and pathologic shape and for group discrimination.

2. METHODS

2.1. Shape representation by spherical harmonics

The SPHARM shape description, originally described by [5], is a hierarchical, global, multi-scale boundary description which is limited to represent objects of spherical topology. The basis functions of the parameterized surfaces are spherical harmonics. A key component of the processing scheme is the mapping of surfaces of volumetric objects to parametrized surfaces prior to expansion into harmonics. Brechbühler [6] presented a solution that initializes a parametric surface net by diffusion between poles and around the meridian and refines the parametrization by nonlinear optimization, solving for area preservation while minimizing distortion of originally squared voxel surface elements. Closed surfaces are thus represented as $\mathbf{v}(\theta,\phi) = (x(\theta,\phi), y(\theta,\phi), z(\theta,\phi))^T$, creating a bijective mapping of the voxel surface to the unit sphere. Object surfaces are thus mapped to the unit sphere and optimized for a homogeneous distribution of parameters. The parametrization of single objects has been later combined with the concept of statistical shape models proposed by Cootes et al. [7, 8], but using the coefficients of the parametrization rather than a point distribution model [9, 2].

2.1.1. Spherical harmonics descriptors

Spherical harmonic basis functions $Y_l^m,\ -l \le m \le l$ of degree l and order m are defined on $\theta \in [0;\pi] \times \phi \in [0;2\pi)$ by the following definitions (see Fig. 2 left for a visualization of the basis function):

$$Y_l^m(\theta,\phi) \quad = \quad \sqrt{\frac{2l+1}{4\pi}\,\frac{(l-m)!}{(l+m)!}}\,P_l^m(\cos\theta)\,e^{im\phi} \quad (1)$$

To express a surface using spherical harmonics, the three coordinate functions are decomposed and the surface $\mathbf{v}(\theta,\phi) = (x(\theta,\phi), y(\theta,\phi), z(\theta,\phi))^T$ takes the form

$$\mathbf{v}(\theta,\phi) = \sum_{l=0}^{\infty}\sum_{m=-l}^{l} \mathbf{c}_l{}^m\, Y_l^m(\theta,\phi)\ , \quad (2)$$

where the coefficients $\mathbf{c}_l^m$ are three-dimensional vectors due to the three coordinate functions. The coefficients $\mathbf{c}_l^m$ are obtained by solving a least-squares problem.

Using spherical harmonic basis functions, we obtain a hierarchical surface description that includes further details as more coefficients are considered (Fig. 2 right).

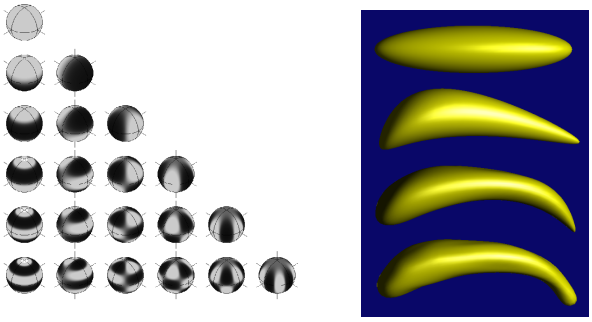

Fig. 2. Decomposition of objects using SPHARM description. Left: Visualization of the Spherical harmonic basis functions. The plot shows the real parts of the spherical harmonic functions Y_l^m, with l growing from 0 (top) to 5 (bottom), and m ranging from 0 (left) to l in each row. Right: Shape representation of a caudate structure (side view) at different degree's; m = 1,2,5,12, top to bottom.

2.1.2. SPHARM correspondence

The scheme for establishing correspondence between object surfaces described by SPHARM [6] is a 3D extension of the 2D arc-length shape parameterization (see also Székely [9]). As the optimal mapping to spherical coordinates and expansion into coefficients does not use any object centered coordinate system, the parameterization needs to be rotated in parameter space for normalization. Our choice is the use of the first order ellipsoid (Fig. 2top right) and the choice of the three major axis as the intrinsic coordinate system. The same coordinates are also used for a spatial aligning of objects by translation and rotation of voxel coordinates. Correspondence between surfaces is therefore defined as the point-to-point correspondence established by points with the same parameter vector (θ_i, ϕ_i). Although our scheme does not use explicit surface features to determine correspondence, visual assessment of meridian lines overlayed on sur-

fces and comparison of coordinates at salient surface locations demonstrate a surprisingly good quality of correspondence. A quantitative evaluation study against manual landmarking and more complex schemes for correspondence optimization is currently in progress.

2.1.3. Shape space

We define a shape space via the population average and its major deformation modes (eigenmodes) determined by a principal component analysis (PCA, Fig 3). We compute the SPHARM shape representations $\vec{c}_i$ for a population and apply PCA to the coefficients as described by Kelemen [2]. The eigenmodes $(\lambda_i, \vec{p}_i)$ in the shape space cover at least 95% of the variability in the population:

$$\Sigma = \frac{1}{n-1}\sum_i (\vec{c}_i - \bar{\vec{c}}) \cdot (\vec{c}_i - \bar{\vec{c}})^T \quad (3)$$

$$0 = (\Sigma - \lambda_i \cdot I_n) \cdot \vec{p}_i; i = 1 \ldots n-1 \quad (4)$$

$$Space_{\text{shape}} = \{\vec{c} \pm 2 \cdot \sqrt{\lambda_i} \cdot \vec{p}_i\}; i = 1 \ldots k_{95\%} \quad (5)$$

Since the shape space is continuous, we need to determine a shape set by a representative sampling of the shape space, either statistically or deterministic. All computations are then applied to this sampled shape set. The number of shapes in this set can be considerably higher than the original number of shapes.

$-2\ \lambda 1$ average $+2\ \lambda 1$

Fig. 3. Shape space defined by PCA: First eigenmode of deformation. The middle, left and right images display the average shape and shape deformations with ± 2 standard deviations. Most evident are the thickness change of the caudate body and the change of bending of the caudate tail.

2.2. Medial Representation

The medial description is computed from a shape space of a training population of objects, represented by surface parameterizations. The topology of the medial description is calculated by studying the topological changes of pruned 3D Voronoi skeletons and establishing a common topology satisfying all the shapes sampled from the shape space. Voronoi skeletons as shape representations have been studied intensively in past by Ogniewicz [11] in 2D, and Naef [12] and Attali [13] in 3D. The major problem for modeling template shapes representative for a population of shapes is the determination of a stable medial model. Besides problems related to biological shape variability, skeletonization schemes are well known to be unstable and sensitive to boundary noise. The new processing scheme developed by Styner et al. [14, 15] presents a novel concept to overcome these limitations. The following description does only summarize the scheme but details can be found in the referenced papers.

The new scheme uses a set of objects sampled from the shape space 2.1.3 and and performs the two steps of computing a common branching topology for pruned Voronoi skeletons and a minimal sampling of the resulting medial manifolds given a predefined maximal approximation error.

2.2.1. Computing a common medial branching topology

The procedure computes the individual branching topology for each member of the shape set and determines the common topology via a spatial matching criterion.

Branching topology of a single shape - The branching topology for a single shape is derived via Voronoi skeletons (see Attali [13]), calculated from a finely sampled PDM representation derived from SPHARM boundary representations. An algorithm for grouping Voronoi faces into sets of medial sheets was developed based on an early concept proposed by Naef [12]. A new merging step follows this initial grouping, merging similar sheets according to a mixed radial and geometric continuity criterion. The computed medial sheets are weighted by their volumetric contribution to the overall object volume: $C_{sheet} = (vol_{skel} - vol_{skel \setminus sheet_i})/vol_{skel}$ and pruned using a topology preserving deletion scheme.

Common spatial frame for branching topology comparison - The problem of comparing branching topologies has already been adressed before in 2D by Siddiqi [16] and others, mainly via matching medial graphs. So far, there is little work done in 3D. Own results in 2D and presented by August [17] have shown that the medial branching topology is quite unstable, which is even more pronounced in 3D. In 3D, the medial branching topology is even more unstable and ambiguous than in 2D. Thus, we chose to develop a matching algorithm that does matching based on spatial correspondence. Our choice for a common spatial frame is the average object of the shape space. We warp each member of the shape set into the common frame using the boundary correspondence given by the PDM. A thin plate spline warping provides a perfect match of the corresponding boundary points while interpolating the warp of the interior skeletons.

Extraction of a common topology - The point sets of the warped skeletons are compared using an overlap criterion based on spatial statistics (mean and second order distribution). Skeleton sheets with high degree of overlap are declared as common sheets, whereas sheets with low degree of overlap among all objects are declared as new sheets of

the common topology model. Iteratively, a common topology model is constructed that represents the topologies of all objects in shape space.

2.2.2. Computing the sampling of the medial manifold

From the common branching topology we compute the sampling of the associated sheets by a grid of medial atoms. To calculate the sampling, we start with the longest 1D axis on the 3D medial sheet and propagate grid points outwards in normal directions to the boundary [15]. The optimal sampling is determined by specifying a maximum approximation error for *all shapes* in the shape space, here the Mean Absolute Distance (MAD) between the implied and original object boundaries. The procedure steps through various sampling grids to finally converge in an optimum. The final m-rep model is then described by the common branching topology and the set of parameters that specify the grid sampling for the medial sheet (see Fig. 1c).

3. RESULTS

We present a processing scheme to build statistical parametric surface and discrete medial models that incorporate information about the population variability, given by a PCA analysis of a training population. Statistical models are essential for segmentation by model-based deformation, as they help to constrain the solution space based on a shape prior. The SPHARM model has been demonstrated with the segmentation of the hippocampus ([2] and for shape description and comparison of brain ventricles in twin studies ([18]). Currently, we are studying the shape variability of the caudate in treatment studies of schizophrenia and are modeling the kidney and liver structures for radiotreatment planning purposes. Whereas SPHARM provides an elegant solution to object alignment and surface correspondence, the set of coefficients is neither intuitive nor robust with respect to local shape changes.

A medial representation captures local width and local curvature separately. Clinicians can thus ask for the nature and intuitive description of shape changes as opposed to global shape changes described by SPHARM. The model building as described above starts from a shape space represented by SPHARM and PDM and derives a medial model that captures the sheet topology of the whole sample set. This is a very important property since the skeleton is subject to topology changes with deformation. The model building on shape populations provides a statistical models for large sets of objects, in our studies up to 200 objects per study, which are used for discriminating healthy versus pathologic or shape change due to aging or treatment, for example. Most encouraging are our studies that show similar shape discrimination of the hippocampus in schizophrenia with SPHARM and M-rep, providing evidence that shape changes, although subtle, are real effects and not artifacts caused by the complex procedure [19, 15].

4. REFERENCES

[1] Christian Brechbühler, *Description and Analysis of 3-D Shapes by Parametrization of Closed Surfaces*, Hartung Gorre, 1995, PhD Dissertation, IKT/BIWI, Swiss Federal Institute of Technology ETH, Zürich, ISBN 3-89649-007-9.

[2] G. Kelemen, A.and Székely and G. Gerig, "Elastic model-based segmentation of 3d neuroradiological data sets," *IEEE Trans. Med. Imaging*, vol. 18, pp. 828–839, October 1999.

[3] S. Pizer, D. Fritsch, P. Yushkevich, V. Johnson, and E. Chaney, "Segmentation, registration, and measurement of shape variation via image object shape," *IEEE Trans. Med. Imaging*, vol. 18, pp. 851–865, Oct. 1999.

[4] S. Joshi, S.M. Pizer, P. T. Fletcher, A. Thall, and G. Tracton, "Multi-scale 3-d deformable model segmentation based on medical description," in *International Conference on Information Processing in Medical Imaging (IPMI)*. 2001, Springer-Verlag.

[5] L.H. Staib and J.S. Duncan, "Deformable Fourier models for surface finding in 3D images," in *VBC'92*, 1992, pp. 90–194.

[6] C. Brechbühler, G. Gerig, and O. Kübler, "Parametrization of closed surfaces for 3-D shape description," *CVGIP: Image Under.*, vol. 61, pp. 154–170, 1995.

[7] T. F. Cootes, A. Hill, C. J. Taylor, and J. Haslam, "The Use of Active Shape Models for Locating Structures in Medical Images," *Image and Vision Computing*, vol. 12, no. 6, pp. 355–366, 1994, Electronic version: http://s10d.smb.man.ac.uk/publications/index.htm.

[8] T. Cootes, C.J. Taylor, D.H. Cooper, and J. Graham, "Active shape models - their training and application," *Computer Vision and Image Understanding*, vol. 61, pp. 38–59, 1995.

[9] G. Székely, A. Kelemen, Ch. Brechbühler, and G. Gerig, "Segmentation of 2-D and 3-D objects from MRI volume data using constrained elastic deformations of flexible Fourier contour and surface models," *Medical Image Analysis*, vol. 1, no. 1, pp. 19–34, 1996.

[10] W. H. Press, S. A. Teukolsky, W. T. Vetterling, and B. P. Flannery, *Numerical Recipes in C*, Cambridge Univ. Press, 2 edition, 1993.

[11] R. Ogniewicz and M. Ilg, "Voronoi skeletons: Theory and applications," in *IEEE Comp. Vision and Pattern Rec.*, June 1992, pp. 63–69.

[12] M. Näf, *Voronoi Skeletons: a semicontinous implementation of the 'Symmetric Axis Transform' in 3D space*, Ph.D. thesis, ETH Zürich, Commmunication Technology Institue IKT/BIWI, 1996.

[13] D. Attali, G. Sanniti di Baja, and E. Thiel, "Skeleton simplification through non significant branch removal," *Image Proc. and Comm.*, vol. 3, no. 3-4, pp. 63–72, 1997.

[14] M. Styner and G. Gerig, "Hybrid boundary-medial shape description for biologically variable shapes," in *Proc. of IEEE Workshop on Mathematical Methods in Biomedical Image Analysis (MMBIA) 2000*, June 2000, pp. 235–242.

[15] Martin Styner and Guido Gerig, "Three-dimensional medial shape representation incorporating object variability," in *Proc. Computer Vision and Pattern Recognition CVPR 2002*. IEEE Computer Society Press, Dec 2002, pp. 651–656.

[16] K. Siddiqi, A. Ahokoufandeh, S. Dickinson, and S. Zucker, "Shock graphs and shape matching," *Int. J. Computer Vision*, vol. 1, no. 35, pp. 13–32, 1999.

[17] J. August, K. Siddiqi, and S. Zucker, "Ligature instabilities in the perceptual organization of shape," in *IEEE Comp. Vision and Pattern Rec.*, 1999.

[18] Guido Gerig, Martin Styner, Jones Douglas, Daniel Weinberger, and Jeffrey Lieberman, "Shape analysis of brain ventricles using spharm," in *Proc. Workshop on Mathematical Methods in Biomedical Image Analysis MMBIA 2001*. IEEE Computer Society, Dec 2001, pp. 171–178.

[19] G. Gerig and M. Styner, "Shape versus size: Improved understanding of the morphology of brain structures," in *Proc. Medical Image Computing and Computer-Assisted Intervention MICCAI2001*, 2001, pp. 24–32.